Frictional force measurement during stick-slip motion of a piezoelectric walker

V Shrikanth*, K R Y Simha† and M S Bobji§
Department of Mechanical Engineering
Indian Institute of Science
Bangalore, India-560012
*Email: vicha@mecheng.iisc.ernet.in †Email: simha@mecheng.iisc.ernet.in
§Email: bobji@mecheng.iisc.ernet.in

***Abstract*—The stick-slip actuator motion is dependent on its natural frequency. The backward motion of the actuator during the slip phase due to the stiffness alters the motion of any stick-slip friction principle based positioners drastically. This work is an attempt to design and fabricate a simple and compact *piezoelectric walker* integrated with a force sensor to measure the frictional force during the slip phase. The underlying idea is to achieve a smooth motion of the walker by understanding the dynamics during slipping.**

I. Introduction

Piezoelectric and piezoceramic actuators and devices are popular because of the small displacements that can be generated with a sub nanometer resolution [1]. Depending on the material, the maximum working range of these actuators are usually a fraction of its length [2]. Long displacements at high travel speeds with a very high resolution are the advantages of stick-slip actuators and drivers [3]. The dynamic range of such systems depend on the driving circuitry rather than the actuator itself.

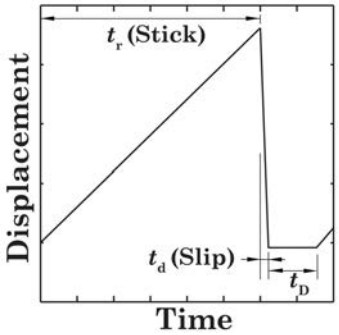

Fig. 1. Different time parameters of the input signal given to the stick-slip actuators [2], [3], [4], [5], [6], [7].

Pohl [8] was the first to utilize the principles of inertia and frictional force to drive a stage, by means of a piezoelectric actuator applied with a sawtooth waveform. The positioning stage was capable of step displacements ranging from 40–200 nm with a travel speed of 200 μm/s. The input signal to the actuator is shown in Fig. 1. The sticking happens during the rise time t_{r}, slipping occurs during the drop time t_{d} and the actuator is at rest during the delay time t_{D}. Niedermann *et al.* [9] utilized the shear deformation generated when a voltage is applied to a piezoelectric plate to drive a stage with the application of stick-slip friction principle. Mamin *et al.* [10] also developed a two dimensional coarse positioner for scanning tunnelling microscope (STM) using piezoceramic actuators. The step size was maintained through closed loop feedback control.

A three dimensional micropositioner using inertial slider principle was developed by Erlandsson *et al.* [11] for use in atomic force microscope (AFM). To obtain vertical motion, Renner *et al.* [12] applied cycloidal waveform to drive the piezo actuator. Spring force made for the normal force necessary for vertical motion. Libioulle *et al.* [13] and Stieg *et al.* [14] developed vertical two dimensional positioners with magnetic force as the source of normal load to move the piezo actuators. Furutani *et al.* [15] showed precise control of displacement by feedback control of the induced charge. Smith *et al.* [16] used impulse force generated by piezo to drive the positioning stage. The traditional Scott-Russell straight line mechanism was included in the positioner design by Chang & Li [5] to get larger step size. Chu & Fan [6] utilized piezo stack actuator to overcome the positioning errors associated with guide rail and bearings used in earlier designs. The friction model as well lumped model of the actuators reported in literature yield a displacement (x_1), velocity ($\dot{x}_1$) and acceleration ($\ddot{x}_1$) as shown in Fig. 2 (a), 2 (b) and 2 (c). From

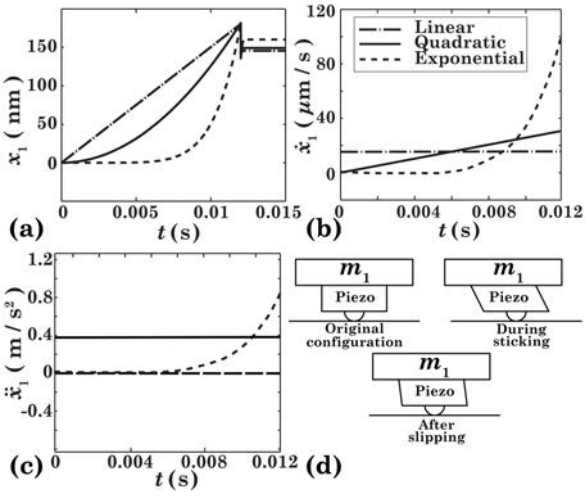

Fig. 2. Walker motion for linear, quadratic and exponential inputs (a) Displacement of the walker, x_1 (b) Velocity, $\dot{x}_1$ (c) Acceleration, $\ddot{x}_1$ (d) Piezo configuration at start, during sticking and after slipping. $t_{\mathrm{r}} = 12$ ms, $t_{\mathrm{d}} = 4\,\mu$s and $t_{\mathrm{D}} = 3$ ms.

a review of the literature related to stick slip actuators, it can be concluded that the with the exception of Bergander

978-1-4799-7800-7/15/$31.00 ©2015 IEEE

and Breguet [4], no other work has been reported that has been an effort to understand the mechanics during slipping. The dynamics of the piezoelectric walker described in this work is an attempt towards comprehending the frequency and amplitude effects as well as influence of friction and frequency of operation of any stick-slip based positioning device.

II. Piezoelectric Walker

A piezoelectric walker shown in Fig. 3 (a) is based on the inertial slider principle. A shear piezoelectric plate (PZT–5A) of sides 5×5 mm and thickness 0.75 mm is sandwiched between copper-beryllium (Cu-Be) electrode plates. The electrode plates are connected to the piezo plate by means of conducting silver epoxy resin and cured at 130° C for 30 minutes. The electrical connections to the electrode plates are made by soldering silver wires (diameter of 150 μm) with polyimide insulation. A thin insulating layer of alumina of thickness 0.15 mm is sandwiched between this assembly and the inertial mass by cyanoacrylate adhesive (Super glue). Another identical assembly is fixed to the actuator piezo assembly separated by an electrically insulating thin alumina layer. Steel spheres of 1 mm diameter are fixed to the electrode plate of the sensor piezo as shown in Fig. 3 (b).

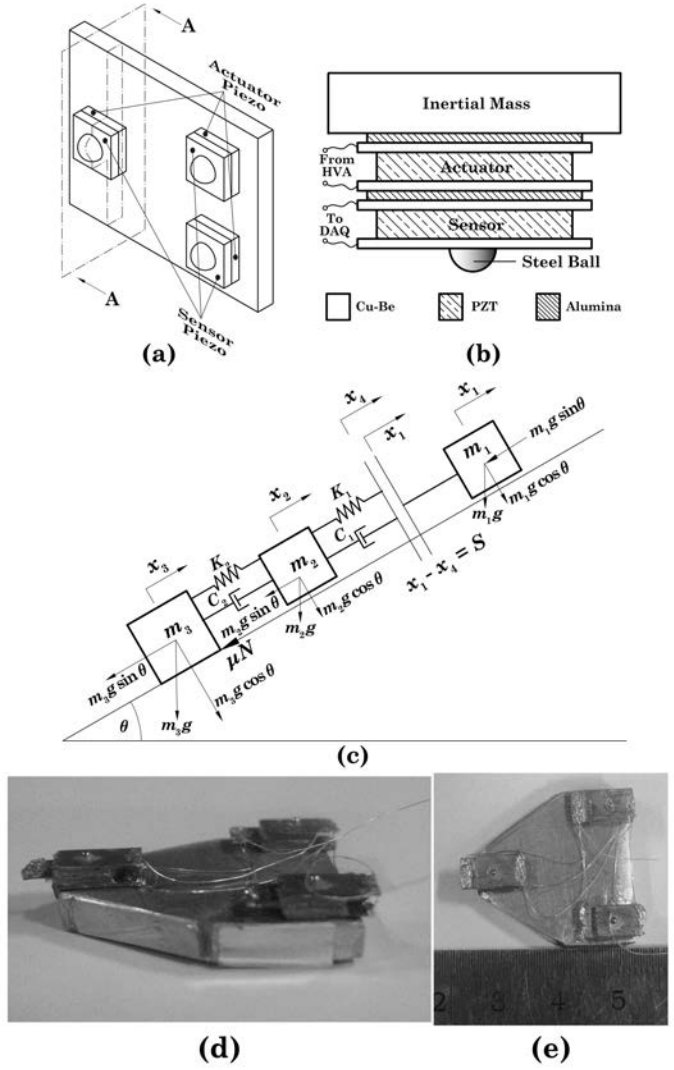

Fig. 3. Piezoelectric walker (a) Geometric model (b) Sectional view of the walker at plane A–A and (c) Lumped model (d) Side view (e) Top view.

A. Working Principle

The piezoelectric walker is designed based on stick-slip effect. Fine motion of the walker can be achieved by proper understanding of the inertial and frictional forces during sticking and slipping. The inertia of the walker is relatively small when the slope of the input waveform dV/dt is low (*i.e.* $a < \mu g$) as shown in Fig. 4 (a). At this moment, the steel balls in contact with the surface stick to it due to static friction while the inertial mass moves. When the slope dV/dt is high ($a > \mu g$), due to the large inertial force the walker begins to slip [5]. The single step motion of the walker is determined by the stick and slip conditions. The walker can be used as a positioner by applying voltage signal periodically. Amplitude, frequency, input waveform type, roughness of the friction surface and inertial mass influence the response of the walker. A magnetic loading system when integrated with the walker increases the driving force by augmenting the contact force to facilitate vertical motion [3]. Compared to an inertial slider in which

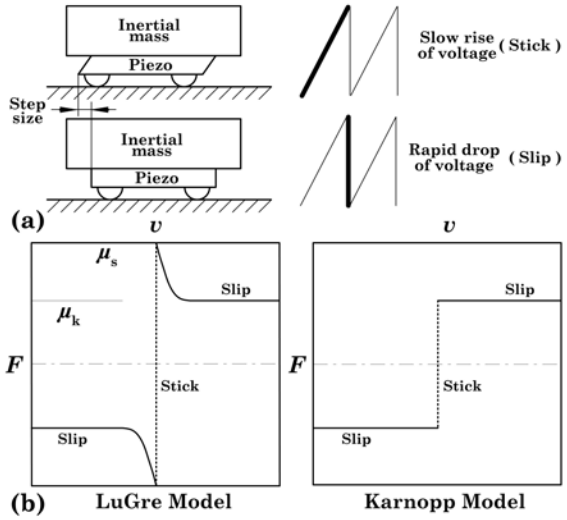

Fig. 4. (a) Schematic for principle of operation (b) Friction models used in modelling the walker.

the legs (piezo sandwich and steel ball) are fixed to a base, the walker has the legs fixed to the inertial mass. As a consequence of this configuration, the motion of the walker is not limited by the length of the inertial mass and can be moved as much as the surface available.

B. Model

The frictional force involved in the stick-slip phenomenon is given by Karnopp model [17] as

$$F = \mathrm{sgn}(v)\left[\mu_{\mathrm{k}}\lambda(v) + \mu_{\mathrm{s}}(1-\lambda(v))\right]N \tag{1}$$

where v is the velocity, μ_{k} and μ_{s} are dynamic and static friction coefficients and $N = (m_1 + m_2)g$ is the normal load. $\lambda(v) = 0$ when $|v| \simeq 0$ and $\lambda(v) = 1$ when $|v| > 0$. Canudas *et al.*[18] proposed the LuGre model by combining Dahl model with steady state friction. Stribeck effect was also included and the resulting model captures frictional lag, stick-slip motion, presliding displacement *etc*.

$$F = \mathrm{sgn}(v)\left[F_{\mathrm{k}} + (F_{\mathrm{s}} - F_{\mathrm{k}})\mathrm{e}^{-\left(\frac{v}{v_{\mathrm{s}}}\right)^2}\right] \tag{2}$$

F_{k} and F_{s} are dynamic and static friction forces, v_{s} is Stribeck velocity. This model was considered for simulating the friction

force influencing the inertial slider motion by Zesch[19], Chu and Fan[6], Fung *et al.*[20]. The equations of motion for the lumped model of the piezoelectric walker given in Fig. 3 (c) are

$$\begin{aligned} m_1\ddot{x}_1 + C_1(\dot{x}_4 - \dot{x}_2) + K_1(x_4 - x_2) + m_1 g\sin\theta = 0 \\ m_2\ddot{x}_2 - C_1(\dot{x}_4 - \dot{x}_2) - K_1(x_4 - x_2) \\ -C_2(\dot{x}_3 - \dot{x}_2) - K_2(x_3 - x_2) + m_2 g\sin\theta = 0 \\ m_3\ddot{x}_3 + C_2(\dot{x}_3 - \dot{x}_2) + K_1(x_3 - x_2) \\ +m_3 g\sin\theta + F = 0 \end{aligned} \quad (3)$$

where $m_1 = 12.7\,\mathrm{g}$ and $m_2 = 5.1\,\mathrm{g}$ and $m_3 = 1.2\,\mathrm{g}$ are the inertial mass, mass of the actuator (piezo, electrode plates and alumina assembly) and mass of the sensor piezo (including the steel sphere) respectively. x_1 is the displacement of the inertial mass, x_2 is the displacement of the actuator and x_3 is the displacement of the sphere fixed to the sensor piezo respectively. $x_4 = x_1 - s$ where $s = d_{15}V(t)$ is the applied displacement to the piezo. d_{15} is the charge constant of the piezo material and $V(t)$ is the input voltage. μ is the coefficient of friction and θ is the inclination angle of the surface. $C_1 = 51.8\,\mathrm{Ns/m}$ and $C_2 = 26.2\,\mathrm{Ns/m}$ are the damping coefficients, $K_1 = K_2 = K = 8 \times 10^8\,\mathrm{N/m}$ are the stiffness of actuator and sensor piezo respectively. x_1 and x_3 are displacements of inertial mass and walker leg (sensor piezo) respectively. The linear input waveform is of the form

$$V(t) = V_0\left(\frac{t}{t_\mathrm{p}}\right) \quad (4)$$

quadratic is

$$V(t) = V_0\left(\frac{t}{t_\mathrm{p}}\right)^2 \quad (5)$$

and exponential is

$$V(t) = \frac{V_0}{2^{15}}\left(\mathrm{e}^{10.39\left(\frac{t}{t_\mathrm{p}}\right)} - 1\right) \quad (6)$$

$\dot{x}_3$ replaces v in (1) and (2) and the frictional force F in (3) can be substituted for, from either (1) or (2). The mass and stiffness matrices are

$$M = \begin{bmatrix} m_1 & 0 & 0 \\ 0 & m_2 & 0 \\ 0 & 0 & m_3 \end{bmatrix}, \quad K\begin{bmatrix} K & -K & 0 \\ -K & 2K & -K \\ 0 & -K & K \end{bmatrix} \quad (7)$$

$|K - M\omega^2| = 0$ is the characteristic equation for the above system of equations. The undamped natural frequencies can be obtained by the solving the characteristic equation. The response of the walker for various input waveforms and a corresponding motion of the walker as well as the frictional force experienced during its motion is presented in the results section.

III. Experimental Setup

The experimental setup consists of the piezoelectric walker which is free to move on a y-stage as shown in Fig. 5 (a). The displacement of the walker is measured by an analog non contact fibre optic reflectance dependent displacement sensor (Philtec D 100) which is mounted on a V-block and fixed on an x-stage. The x-stage and y-stage are used to align the displacement sensor tip and piezoelectric walker. The entire assembly is fixed on a vibration isolation table. The DC voltage

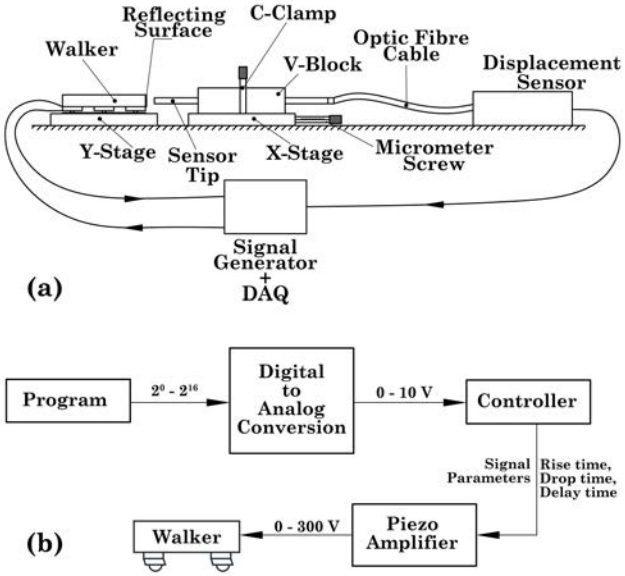

Fig. 5. (a) Schematic of the experimental setup (b) Block diagram of the signal generator.

output from the displacement sensor is recorded by a National Instruments (NI) data acquisition card (DAQ) (PCIe 6363).

A computer interfaced with a 16-bit digital to analog converter generates the necessary signal to drive the walker as shown in Fig. 5 (b). This signal is amplified by a high voltage piezo amplifier to boost the waveform upto 300 V. The walker is driven by this amplified signal. The signal parameters such as rise time (t_r), drop time (t_d) and delay time (t_D) can be set to any value by the controller. Linear, quadratic and exponential waveforms are used as input signals for investigating the motion of the walker. The walker moves when it is excited by any of the three waveforms gradually from 0–300 V and abruptly decreased to 0 V due to stick-slip effect.

IV. Results

The parameters involved in determining the performance of the piezoelectric walker are coefficient of friction μ, inclination angle θ, inertial mass m_1 and input signal amplitude V_0. The coefficient of friction can be varied by using suitable lubricants as well as different contact pairs (sapphire ball; steel, glass, aluminum base *etc.*). The base of the platform can be tilted to vary the inclination angle. The default values are $\mu = 0.26$ (Al alloy-steel), $m_1 = 12.7\,\mathrm{g}$ and $V_0 = 300\,\mathrm{V}$. The inclination of the walker base is kept horizontal in this study ($\theta = 0$ for all the simulations and experiments).

A. Numerical simulation

Fig. 6 shows the applied input signal,displacement of the walker and the frictional force measured by the sensor piezo for linear, quadratic and exponential input waveform respectively. The applied voltage is converted to a displacement according to the relation $s = d_{15}V$. This input displacement moves the walker by a distance x_1. The motion of the walker due to an input signal is possible due to stick-slip effect. As the actuator elastically recovers, the sensor piezo is moved on the contact surface. Thus, the sensor piezo is deformed during the retraction and hence a charge is developed. The sensor piezo is

represented by m_3 in the lumped model shown in Fig. 3 (c).The charge developed in the sensor piezo due to its displacement is $\Delta x = x_3 - x_2$, which is the relative displacement of the sensor piezo. The frictional force F is equal to a restoring spring force of the sensor piezo $F_{\rm s} = K\Delta x$. The voltage output of the sensor piezo is $V_{\rm out} = (\Delta x\, \mathfrak{C}/d_{15}) \times S$ where S is the sensitivity of the inline charge amplifier used in the data acquisition and $\mathfrak{C}$ is the capacitance of the sensor piezo. The

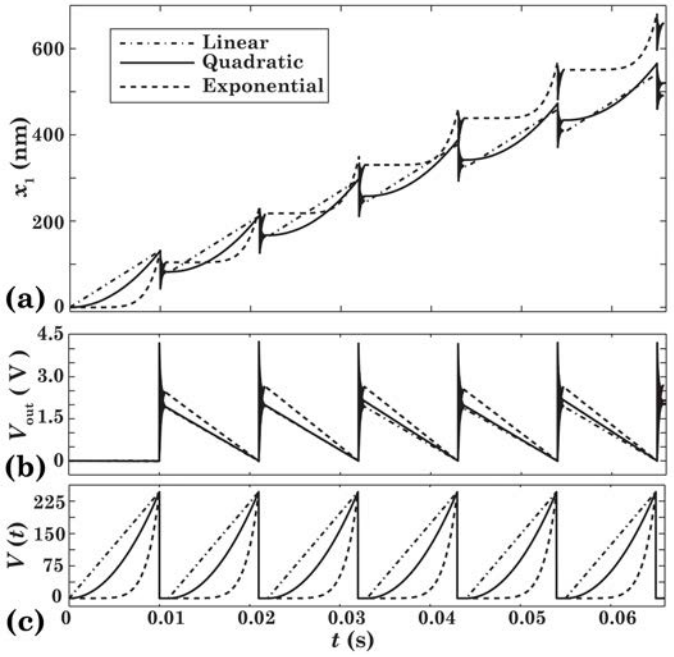

Fig. 6. Numerical simulation of the response of the walker for linear, quadratic and exponential input waveforms; (a) Inertial mass displacement x_1 (b) The output voltage of the sensor piezo which is a measure of the frictional force experienced by the walker (c) Applied input voltage $V(t)$. $\mu = 0.26$, $\theta = 0°$, $V_0 = 225\,\mathrm{V}$, $t_{\rm r} = 10\,\mathrm{ms}$, $t_{\rm d} = 4\,\mu\mathrm{s}$ and $t_{\rm D} = 1\,\mathrm{ms}$.

variation in the step size of the walker for the three waveforms is shown in Fig. 6 (a). The linear, quadratic and exponential waveforms displaces the walker by the same amount during the sticking phase. But, because of the sudden drop, the walker undergoes a backward motion and the net displacement is less than the applied displacement. The walker has the highest velocity and acceleration when exponential waveform is applied (Fig. 2 (b) and 2 (c)). The step size is dependent on the velocity just before the slip starts to occur. For any waveform, the sharp drop in the input voltage during the slipping phase is exponential. The walker leg lags behind the inertial mass which depends on coulomb and viscous (lubricant use) damping. Also, due to very high acceleration during the drop in voltage, the inertial mass is moved slightly backward and the motion decays exponentially as shown in Fig. 2 (a).

B. Experimental results

Fig. 7 shows the experimental results of the response of the walker for linear, quadratic and exponential input waveforms. The motion of the walker for the three input waveforms is presented in Fig. 7 (a). The displacement of the walker is maximum per cycle when the input waveform is exponential. The quadratic waveform gives a displacement slightly higher than that for a linear input. The exponential waveform gives a

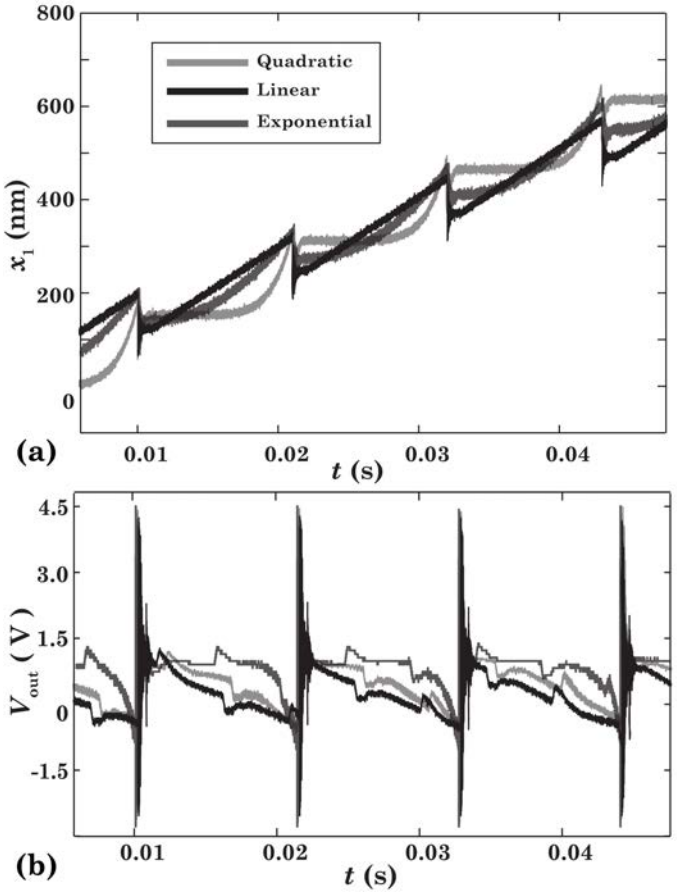

Fig. 7. Experimental evidence of the motion of the walker for linear, quadratic and exponential input waveforms; (a) Displacement of the walker corresponding to an input displacement (b) Force measured by the sensor piezo during the motion of the walker is also presented. $\mu = 0.26$, $\theta = 0°$, $V_0 = 225\,\mathrm{V}$, $t_{\rm r} = 10\,\mathrm{ms}$, $t_{\rm d} = 4\,\mu\mathrm{s}$ and $t_{\rm D} = 1\,\mathrm{ms}$.

step size that is 10 % more than the other two input waveforms. Fig. 7 (b) shows the voltage output of the sensor piezo during the motion of the walker. The voltage is almost 1.5 times the applied input voltage during the slip phase. As the actuator piezo elastically recovers after the sudden retraction of the walker leg during slipping, the sensor piezo discharges to give an output voltage nearly equal to the initial value. Due to the residual deformation of the sensor piezo (similar to shown in 2 (d)) after slipping, some residual voltage is measured as the output from the sensor piezo.

The inertial mass (m_1) determines the walker motion for two reasons: (a) resistance to high acceleration during the slipping phase; and (b) normal load and hence the frictional load at point of contact. With increase in m_1, the frictional force experienced by the steel sphere (contact point) proportionately increases. As a consequence of this, the piezo will not completely retract during the slipping phase and some residual elastic deformation of the piezo element will exist as shown in Fig. 2 (d). When the acceleration is zero [8], the frictional force becomes zero while the walker leg sticks to the surface below.

The rise time, drop time and delay time of the input signal determines the velocity and acceleration of the walker. As the rise time and drop time are reduced, the velocity

and acceleration increases. Thus the step size of the walker is increased with decreasing t_{r} and t_{d}. The delay time (t_{D}) determines the magnitude of the backward motion of the walker. When the next ramp is delayed, the inertial mass starts to move backwards [4]. The dynamics of the walker are explained in detail in the next section concentrating on the force measurement done during the slipping phase for all three input waveforms.

V. Discussion

The slipping occurs due to rapid retraction of the actuator piezo when the input voltage is suddenly dropped to zero. At the end of the input ramp as shown in Fig. 1, the velocity of the walker is highest for any input waveform. In case of exponential waveform, the acceleration also needs to be considered since it varies continuously with time. As the input

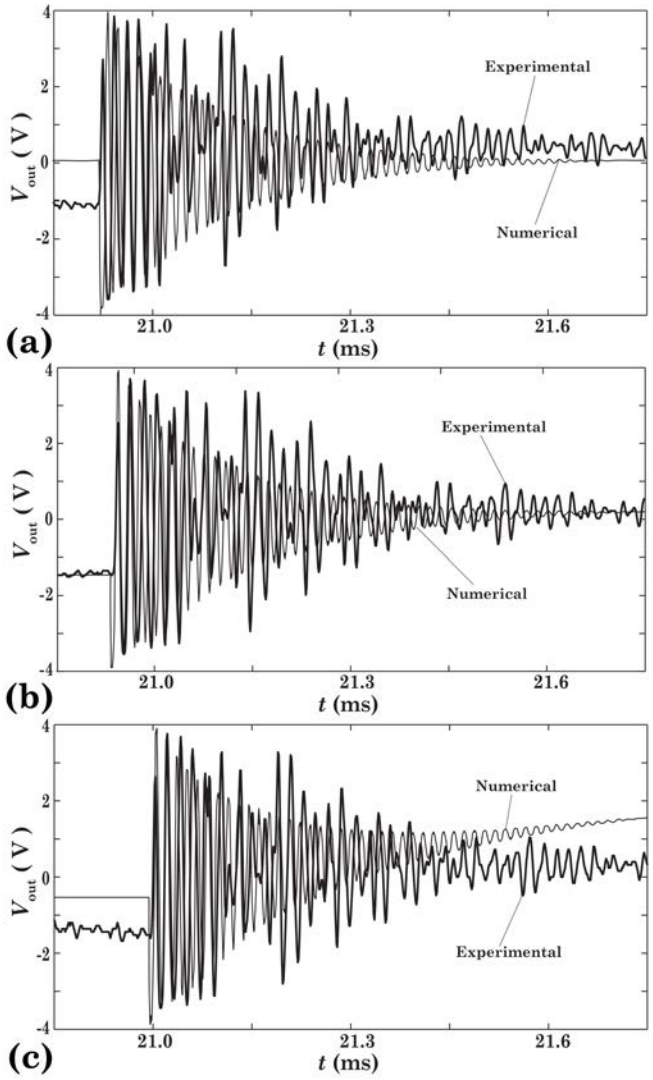

Fig. 8. The response of the sensor piezo during the slip phase of the walker motion; Numerical and experimental measurement of the voltage output for (a) Linear input (b) Quadratic input and (c) Exponential input waveforms.

voltage begins to drop suddenly, there is a reversal in the direction of velocity and acceleration. Given the short duration for which slipping occurs, the smooth motion of the walker is next to impossible without suitable compensations in its construction that might turn out to be a complex design. The jerky motion of the walker can be avoided if one can understand the dynamics of it to achieve better motion and positioning.

It is observed that as the coefficient of friction is reduced, the average step size reduces. The piezo shears and the mass moves when the signal is applied during t_{r} (Fig. 1 (b)). The mass will have some finite velocity and continues to move even when the input voltage drops to zero and hence does not immediately come to its original configuration. The mass oscillates and comes to rest after some time. Generally, any reduction in μ corresponds to a reduction in the step size. When the inertial mass (m_1) is kept constant, any reduction in μ results in lesser chance of the walker to stick to the surface during t_{r}. This is reflected in the net reduced displacement.

Fig. 8 shows the numerical and experimental response of the sensor piezo during the slip phase of the motion of the walker. The sudden drop in the input voltage retracts the actuator piezo. This retraction moves the walker leg with the sensor piezo at very high velocity thus generating a charge in the piezo corresponding to its displacement relative to that of the actuator. Fig. 8 (a), 8 (b) and 8 (c) are the voltage output of the sensor piezo for linear, quadratic and exponential waveforms respectively. The response during the slip phase of the results shown in Fig. 7 (b) for all three waveforms are presented in Fig. 8. The response of the sensor piezo is quite similar for all the three waveforms during the slip phase. The numerical results are in good agreement with the experimentally obtained ones and the amplitude of the oscillations are independent of the input waveform type. It is very important to mention here that the amplitude and the frequency of the oscillations shown in Fig. 8 are dependent on the stiffness of the piezo material used. The amplitude of the decaying oscillations is also dependent on the amplitude of the voltage drop of the input signal.

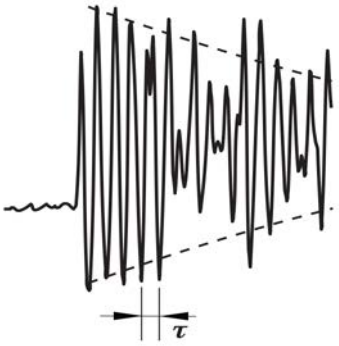

Fig. 9. Voltage output of the sensor piezo during the slip phase for the initial oscillations to determine the damped natural frequency.

Fig. 9 shows the results shown in Fig. 8 during the first 15 oscillations of the actuators piezo. The voltage measured along with the time data can be used to determine one of the natural frequencies of the walker. For this design of the walker, the natural frequency arrived at, after analyzing the results in Fig. 9 might be a combination of the the natural frequencies of both actuator and sensor piezos respectively. As can be seen from Fig. 9, the response has atleast two frequency

components giving rise to beat phenomenon just after the slip occurs. The time interval between two peaks as shown in Fig. 9 is $\tau \sim 20\,\mu$s and hence one of the damped natural frequency is $f_{\mathrm{d}} \sim 50\,$kHz. Any stick-slip based actuator cannot be driven at very high velocities because of two reasons: (1) either they have a very short stroke length due very high stiffness or (2) Very low natural frequencies and hence a large displacement. In this case, the masses m_1, m_2 and m_3, damping ratio due to both coulomb and viscous damping and the natural frequency of the walker determine the maximum operating frequency.

Further research is ongoing to optimize the other parameters such as velocity ($\dot{x}_1$), acceleration ($\ddot{x}_1$) and jerk ($\dddot{x}_1$). Also, determination of the dynamic coefficient of friction μ_{k} during the slipping phase which would be quite different from the static coefficient of friction μ_{s} and hence coulomb damping and its effects on slipping is in progress. It is important to emphasize here that stick-slip piezoelectric walker response is a nonlinear phenomenon exhibiting jerky motion during the slip phase, which is discrete in nature. In addition to this, there is the continuous motion during the stick phase. This discrete to continuous mode transition requires further considerations of frequency and amplitude effects. There is also a need to control the undesirable effects of yaw and drift to achieve superior positioning performance of the piezoelectric walker.

VI. Conclusion

An inertial slider principle based piezoelectric walker is developed to be used in micro and nano positioning systems. The advantage of this piezoelectric walker is that it can be moved on a base or a platform without any restriction on the length of travel. The walker can be moved by any periodic waveform as long as the input amplitude is slowly increased and then suddenly dropped to zero. The displacement of the walker is highest when exponential ramp input is applied. The walker design presented here can be extended to mass with large lateral area. This walker is integrated with a sensor piezo that can measure the frictional force during the motion of the walker. The simplicity of the design and small number of components involved in its construction makes it advantageous and reliable to study the dynamics of the walker; from discrete to continuous transition during its motion.

Acknowledgment

The authors are grateful to K Anantheshwara, N S Murali, Ajay Kumar Panda and Sulochana E K of Force Microscopy Lab, Department of Mechanical Engineering, Indian Institute of Science, Bangalore. The authors are also thankful to Robert Bosch Centre for Cyber-Physical Systems (RBCCPS) for partly funding this project.

References

[1] A. Holman, P. Scholte, W. C. Heerens, and F. Tuinstra, "Analysis of piezo actuators in translation constructions," *Review of scientific instruments*, vol. 66, no. 5, pp. 3208–3215, 1995.

[2] A. Bergander, J.-M. Breguet, C. Schmitt, and R. Clavel, "Micropositioners for microscopy applications based on the stick-slip effect," in *Micromechatronics and Human Science, 2000. MHS 2000. Proceedings of 2000 International Symposium on*. IEEE, 2000, pp. 213–216.

[3] J.-M. Breguet and R. Clavel, "Stick and slip actuators: design, control, performances and applications," in *Micromechatronics and Human Science, 1998. MHS'98. Proceedings of the 1998 International Symposium on*. IEEE, 1998, pp. 89–95.

[4] A. Bergander and J.-M. Breguet, "Performance improvements for stick-slip positioners," in *Micromechatronics and Human Science, 2003. MHS 2003. Proceedings of 2003 International Symposium on*. IEEE, 2003, pp. 59–66.

[5] S. Chang and S. Li, "A high resolution long travel friction-drive micropositioner with programmable step size," *Review of Scientific Instruments*, vol. 70, no. 6, pp. 2776–2782, 1999.

[6] C.-L. Chu and S.-H. Fan, "A novel long-travel piezoelectric-driven linear nanopositioning stage," *Precision Engineering*, vol. 30, no. 1, pp. 85–95, 2006.

[7] J.-L. Ha, R.-F. Fung, C.-F. Han, and J.-R. Chang, "Effects of frictional models on the dynamic response of the impact drive mechanism," *Journal of vibration and acoustics*, vol. 128, no. 1, pp. 88–96, 2006.

[8] D. W. Pohl, "Dynamic piezoelectric translation devices," *Review of Scientific Instruments*, vol. 58, no. 1, pp. 54–57, 1987.

[9] P. Niedermann, R. Emch, and P. Descouts, "Simple piezoelectric translation device," *Review of scientific instruments*, vol. 59, no. 2, pp. 368–369, 1988.

[10] H. J. Mamin, D. W. Abraham, E. Ganz, and J. Clarke, "Two-dimensional, remote micropositioner for a scanning tunneling microscope," *Review of scientific instruments*, vol. 56, no. 11, pp. 2168–2170, 1985.

[11] R. Erlandsson and L. Olsson, "A three-axis micropositioner for ultrahigh vacuum use based on the inertial slider principle," *Review of scientific instruments*, vol. 67, no. 4, pp. 1472–1474, 1996.

[12] C. Renner, P. Niedermann, A. Kent *et al.*, "A vertical piezoelectric inertial slider," *Review of scientific instruments*, vol. 61, no. 3, pp. 965–967, 1990.

[13] L. Libioulle, A. Ronda, I. Derycke, J. Vigneron, and J. Gilles, "Vertical two-dimensional piezoelectric inertial slider for scanning tunneling microscope," *Review of scientific instruments*, vol. 64, no. 6, pp. 1489–1494, 1993.

[14] A. Stieg, P. Wilkinson, and J. Gimzewski, "Vertical inertial sliding drive for coarse and fine approaches in scanning probe microscopy," *Review of scientific instruments*, vol. 78, no. 3, p. 036110, 2007.

[15] K. Furutani, M. Urushibata, and N. Mohri, "Displacement control of piezoelectric element by feedback of induced charge," *Nanotechnology*, vol. 9, no. 2, p. 93, 1998.

[16] A. Smith, S. Gwo, and C. Shih, "A new high-resolution two-dimensional micropositioning device for scanning probe microscopy applications," *Review of scientific instruments*, vol. 65, no. 10, pp. 3216–3219, 1994.

[17] D. Karnopp, "Computer simulation of stick-slip friction in mechanical dynamic systems," *Journal of dynamic systems, measurement, and control*, vol. 107, no. 1, pp. 100–103, 1985.

[18] C. Canudas de Wit, H. Olsson, K. Aström, and P. Lischinsky, "A new model for control of systems with friction," *IEEE Transactions on automatic control*, vol. 40, no. 3, pp. 419–425, 1995.

[19] W. Zesch, "Multi-degree-of-freedom micropositioning using stepping principles," Ph.D. dissertation, Diss. Techn. Wiss. ETH Zürich, Nr. 12318, 1997. Ref.: G. Schweitzer; Korref.: RY Siegwart, 1997.

[20] R.-F. Fung, C.-F. Han, and J.-L. Ha, "Dynamic responses of the impact drive mechanism modeled by the distributed parameter system," *Applied Mathematical Modelling*, vol. 32, no. 9, pp. 1734–1743, 2008.